This article was downloaded by: [University of Utah], [Michael Zhdanov]
On: 07 October 2011, At: 13:16
Publisher: Taylor & Francis
Informa Ltd Registered in England and Wales Registered Number: 1072954 Registered office: Mortimer House, 37-41 Mortimer Street, London W1T 3JH, UK

Inverse Problems in Science and Engineering
Publication details, including instructions for authors and subscription information:
http://www.tandfonline.com/loi/gipe20

Source characterization of atmospheric releases using stochastic search and regularized gradient optimization

B. Addepalli [a], K. Sikorski [b], E.R. Pardyjak [a] & M.S. Zhdanov [c]

[a] Department of Mechanical Engineering, University of Utah, Salt Lake City 84112, USA

[b] School of Computing, University of Utah, Salt Lake City 84112, USA

[c] Department of Geology and Geophysics, University of Utah, Salt Lake City 84112, USA

Available online: 28 Jun 2011

To cite this article: B. Addepalli, K. Sikorski, E.R. Pardyjak & M.S. Zhdanov (2011): Source characterization of atmospheric releases using stochastic search and regularized gradient optimization, Inverse Problems in Science and Engineering, DOI:10.1080/17415977.2011.589901

To link to this article: http://dx.doi.org/10.1080/17415977.2011.589901

PLEASE SCROLL DOWN FOR ARTICLE

Full terms and conditions of use: http://www.tandfonline.com/page/terms-and-conditions

This article may be used for research, teaching, and private study purposes. Any substantial or systematic reproduction, redistribution, reselling, loan, sub-licensing, systematic supply, or distribution in any form to anyone is expressly forbidden.

The publisher does not give any warranty express or implied or make any representation that the contents will be complete or accurate or up to date. The accuracy of any instructions, formulae, and drug doses should be independently verified with primary sources. The publisher shall not be liable for any loss, actions, claims, proceedings,

demand, or costs or damages whatsoever or howsoever caused arising directly or indirectly in connection with or arising out of the use of this material.

Downloaded by [University of Utah], [Michael Zhdanov] at 13:16 07 October 2011

Inverse Problems in Science and Engineering
2011, 1–28, iFirst

Downloaded by [University of Utah], [Michael Zhdanov] at 13:16 07 October 2011

Source characterization of atmospheric releases using stochastic search and regularized gradient optimization

B. Addepalli[a], K. Sikorski[b], E.R. Pardyjak[a]* and M.S. Zhdanov[c]

[a]*Department of Mechanical Engineering, University of Utah, Salt Lake City 84112, USA;*
[b]*School of Computing, University of Utah, Salt Lake City 84112, USA;*
[c]*Department of Geology and Geophysics, University of Utah, Salt Lake City 84112, USA*

(*Received 31 March 2010; final version received 13 May 2011*)

In this work, an inversion technique comprising stochastic search and regularized gradient optimization is used to solve the atmospheric source characterization problem. The inverse problem comprises retrieving the spatial coordinates, source strength and the wind speed and wind direction at the source, given certain receptor locations and concentration values at these receptor locations. The Gaussian plume model is adopted as the forward model and derivative-based optimization is chosen to take advantage of its simple analytical nature. A new misfit functional that improves the inversion accuracy of atmospheric inverse-source problems is developed and is used in the solution procedure. Stochastic search is performed over the model parameter space to identify a good initial iterate for the gradient scheme. Several Quasi-Monte Carlo point-sets are considered in the stochastic search stage and their performance is evaluated against the Mersenne–Twister pseudorandom generator. Newton's method with the Tikhonov stabilizer and adaptive regularization with quadratic line-search is implemented for gradient optimization. As the forward modelling and measurement errors for atmospheric inverse problems are usually unknown, issues concerning 'model-fit' and 'data-fit' are examined. In this article, the workings and validation of the proposed approach are presented using field data from the Copenhagen tracer experiments.

Keywords: inverse-source problem; Gaussian plume model; Monte Carlo; Quasi-Monte Carlo; regularized Newton's method; quadratic line-search

AMS Subject Classifications: 15A29; 11K45; 60J60

1. Introduction

The solution of inverse problems involves the retrieval of information about a physical process or phenomenon from known or observed data [1]. Inverse problems arise in various fields and hence techniques to solve such problems have been an area of extensive study. One of the contemporary applications of inversion techniques includes the source characterization problem for atmospheric contaminant dispersion. Atmospheric source characterization problems, also referred to as event reconstruction, source-inversion or

*Corresponding author. Email: pardyjak@eng.utah.edu

ISSN 1741–5977 print/ISSN 1741–5985 online
© 2011 Taylor & Francis
DOI: 10.1080/17415977.2011.589901
http://www.informaworld.com

inverse-source problems, comprise characterizing the source of a chemical/biological/radiological (CBR) agent released into the atmosphere. Source characterization typically involves predicting the release location and rate of the CBR agent and the meteorological conditions at the release site, based on the time-averaged concentration and wind measurements obtained from a distributed sensor network in the region of interest. In this article, an inversion technique developed to retrieve the spatial coordinates, source strength and the wind speed, and wind direction at the source, using concentration measurements from known receptor locations in the domain is described.

Efficient and robust event reconstruction tools can play a crucial role in the event of accidental or deliberate release of CBR agents in or close to urban centres. Under such circumstances, quick and accurate reconstruction can help government agencies evacuate people from the affected regions. Also, using the information obtained from inversion, forward models can be run to estimate the extent of the plume spread and the consequent exposure. Event reconstruction tools can also be of use to environmental monitoring agencies as they can help evaluate the contribution of the stack releases from various industries close to urban areas to the air quality within urban areas. Therefore, from the perspective of public safety and national security, a fast, robust and accurate atmospheric event reconstruction tool is pivotal for air-quality management and to effectively deal with emergency response scenarios.

It is generally well-accepted that a single best procedure to solve an inverse problem does not exist. For inverse problems having small domains and few decision variables, conducting an exhaustive grid search is the most robust inversion technique [2]. For larger problems, the performance of a solution technique depends upon the problem at hand, the nature of the forward model, and the manner in which the inverse problem is formulated. Inverse problems are also difficult to solve owing to their inherent ill-posedness, i.e. the existence, uniqueness and stability of the computed solution. For real-life inverse problems, the question of existence is more mathematical than physical [1,3]. This is also true for the present case, wherein the sensor network recording a measurement suggests the existence of a solution to the source characterization problem. However, to date, there is no formal proof for the existence of solutions to inverse problems with contaminated data, and seldom do we obtain noise-free data from measuring devices [3]. Therefore, for the accurate retrieval of the model parameters (m), the knowledge of the uncertainty in the observed data (d_{obs}) is absolutely essential. In short, one needs to know the uncertainties (δ) in the data to know what it means to fit the data [3].

The solution phase of inverse problems can be divided into two stages [3]: (1) the estimation stage, and (2) the appraisal stage. The estimation stage involves using an inversion algorithm to predict a set of model parameters (m_{pr}) based on the observed data (d_{obs}). The appraisal stage is comprised of determining how well the data generated (d_{pr}) using the predicted model parameters (m_{pr}) fits the observed data (d_{obs}) [1]. Errors arising in inversion and the inherent ill-posedness associated with inverse problems can be accounted for in one of these two stages. Errors arising in the inversion procedure can be attributed to one of the four possible sources: (1) the forward modelling error (δ_{FM}), (2) measurement error (δ_{M}), (3) non-uniqueness and (4) nonlinear error propagation. For real-life problems, the forward modelling error (δ_{FM}) is inevitable. This is because no forward model (A) can ever incorporate all the physics associated with the problem. During inversion, the forward modelling (δ_{FM}) and the measurement errors (δ_{M}) may be accounted for in the estimation stage. Non-uniqueness arises primarily due to one of the following four factors: (1) retrieval of a model that may have infinite degrees of freedom

Downloaded by [University of Utah], [Michael Zhdanov] at 13:16 07 October 2011

Downloaded by [University of Utah], [Michael Zhdanov] at 13:16 07 October 2011

from finite amount of data, (2) lack of information – this is especially true when solving an under-determined system, (3) correlation between the model parameters (m) and (4) distortion of the misfit functional space due to the previously mentioned errors resulting in multiple optimal solutions. Non-uniqueness and nonlinear error propagation (that is intractable) can be accounted for during the appraisal stage. Due to these uncertainties in the solution procedure, one usually defines a 'data-fit' or 'model-acceptancy' criterion (β) based on any prior information available about the noise level (δ) [4–7]. In summary, the goal of inversion is to find a set of model parameters (m_{pr}) that fit the observed data (d_{obs}) to some prescribed level (β).

Given that the subject of source characterization of atmospheric contaminant dispersion is in its infancy, researchers have examined the applicability and effectiveness of the various available inversion procedures to solve such problems. The solution methodologies used span the range of deterministic (adjoint methods), stochastic (simulated annealing (SA), genetic algorithms (GA), Bayesian inference using Markov Chain Monte Carlo (MCMC) sampling) and 'common-sense' methods (collector footprint methods). The inverse-source problem has been solved over local [8,9], regional [10,11] and continental scales [12] for different model parameters (m) using empirical, diagnostic and prognostic models for scalar transport as the forward operator (A). Apart from identifying the source parameters, inversion techniques have also been used to estimate model coefficients in forward operators used to characterize atmospheric dispersion [12,13]. Table 1 summarizes the salient features of the inversion procedures adopted by some of the research groups across the world to solve the inverse-source problem.

All inversion techniques have their own merits and demerits and the approaches found in Table 1 are no exception. Adjoint methods, apart from requiring a good initial guess, also require the misfit functional to be continuous and differentiable. Hence, they are more likely to get trapped in local minima since inverse problems are often characterized by misfit functionals that have multiple critical points (maxima, minima and saddle points). Also, for problems that have complicated forward operators in the form of partial differential equations (PDEs), adjoint methods can be computationally expensive as they require the forward model evaluation and the Frechet evaluation over the entire domain on every iteration (when Newton's method is employed, evaluation of the inverse of the Hessian over the entire domain is required). Therefore, problems that have complicated (non-convex) misfit functional surfaces often require stochastic search methods in order to distinguish the local minima from the global minima. The computational efficiency of guided-search algorithms such as SA and GA also depends on the forward operator, as every iteration of these algorithms requires the forward operator to be evaluated. Adjoint methods, SA and GA also carry the added disadvantage that they only provide a single model that fits the data rather than giving a set of acceptable models. Though Bayesian inference techniques appear robust and give probabilistic answers, they rely heavily upon the manner in which prior information is included into the initial probability distribution [14]. The posterior distribution is then computed using MCMC sampling, which also requires the forward model to be evaluated on every iteration, and hence can get computationally intractable in higher dimensions [3].

In this article, an approach that has the combined benefits of stochastic search and gradient descent methods is presented. The workings of the proposed approach are explained using field experiment data (the Copenhagen tracer experiments – TCTE) [15]. The objective of conducting stochastic search is to provide the gradient optimization scheme a good starting solution (m_{STOCH}). It should be noted that the stochastic search is

Downloaded by [University of Utah], [Michael Zhdanov] at 13:16 07 October 2011

Table 1. Salient features of various inversion techniques used to solve atmospheric source characterization problems.

Ref.	Model parameters (m)	Forward model (A)	Inversion technique	Validation procedure	Application	Performance
[10]	Q_s	Steady laminar incompressible Navier-Stokes solver + ADE	Adjoint method	Synthetic data without noise	Contamination dispersion	
[16]	x_s, y_s, z_s, Q_s, u_s, θ_s, δ_s	Gaussian puff	GA	Synthetic data without noise	Atmospheric source inversion	
[17]	x_s, y_s, Q_s	GPM	Detector footprint method	Synthetic data with and without noise	Atmospheric source inversion	
[8]	x_s, y_s, z_s, Q_s	FEM3MP – 3D	Bayesian inference + MCMC	Synthetic and field data	Atmospheric source inversion	(1) 2560 forward runs (2) Total computation time: over 12 h on 1024 2.4 GHz Xeon processors
[11]	z_s, t_s	Chemistry transport model – POLAIR 3D	Adjoint method		Reconstruction of Chernobyl accident source term	
[18]	x_s, y_s, Q_s, u_s, θ_s,	GPM	GA	Synthetic data without noise	Atmospheric source inversion	(1) 2000 generations meteorological parameters

Downloaded by [University of Utah], [Michael Zhdanov] at 13:16 07 October 2011

	stability class					(2) 10,000 generations for x_s, y_s, Q_s, θ_s & stability
[12]	$f_{j,m}$, s_{OH}, s_{stea}, c_0	Global atmospheric CTM	Adjoint method	Field data	Global-scale sources & sinks of methane	
[19]	x_s, y_s, z_s, Q_s	GPM	Expectation maximization	Synthetic data without noise	Atmospheric source inversion	
[20]	x_s, y_s, Q_s, θ_s	Gaussian puff	GA + simplex optimization	Synthetic data without noise		(1) 1200 chromosomes (2) 100 GA iterations
[21]	Q_s	Langevin model	Quasi-Newton and SA	Field data	Atmospheric source inversion	(1) 65 quasi-Newton iterations (2) 1575 SA iterations
[9]	x_s, y_s, z_s, Q_s, u_s, θ_s	GPM	Bayesian inference + MCMC	Field data	Atmospheric source inversion	50,000 MCMC evaluations
[13]	K_{xx}, u_*, L, z_0	2D ADE	Levenberg–Marquardt method	Field data	Identification of atmospheric boundary layer parameters	
[22]	x_s, y_s, z_s, Q_s	GPM	SA	Field data	atmospheric ethane used to locate ground-level sources	4×10^6 iterations

Note: t_s – temporal release profile, $f_{j,m}$ – integrated surface emission over region j & month m, s_{OH} – parametrization for chemical removal of methane with hydroxyl radical, s_{stea} – stratospheric methane loss, c_0 – global mean methane concentration, K_{xx} – longitudinal turbulent diffusivity, u_* – friction velocity, L – Monin-Obukhov length, z_0 – aerodynamic surface roughness, CTM – chemistry transport model, GPM – Gaussian plume model, SA – simulated annealing, ADE – advection–diffusion equation, GA – genetic algorithm.

not a guided-search and this ensures that the misfit functional space has been uniformly sampled, thereby reducing the possibility of getting stuck in local minima. Three strategies for solving the inverse-source problem in general and computing the 'data-fit' criterion (β_{STOCH}) for the stochastic search stage in particular are discussed. Gradient optimization (Newton's method) is performed with the initial iterate provided by the stochastic search stage (m_{STOCH}). The 'model-acceptancy' criterion (β_{GD}) for the gradient scheme is based on the L_2-norm of the difference between predicted and observed data vectors in the iteration space. The Gaussian plume dispersion model is adopted as the forward model because of its theoretical and computational simplicity. The proposed approach is used to retrieve the source parameters from TCTE [15], and the results obtained are compared against the true parameters. The works of [9,21] also used the Copenhagen data to demonstrate quasi-Newton and Bayesian inference approaches to the inverse problem. The results obtained from this work are compared to those obtained by [9,21].

Apart from the hybrid approach proposed, this article also investigates some of the vital aspects of the atmospheric source characterization problem when using the Gaussian plume model (GPM) as the forward operator. The first feature examined is the effect of the misfit functional formulation on the accuracy and complexity of inversion. Based on this study, a new misfit functional that takes into account both the zero and non-zero measurements recorded by the receptors and improves the inversion accuracy of atmospheric inverse-source problems is developed and is used in the solution procedure. Several Quasi-Monte Carlo (QMC) point-sets are considered in the stochastic search stage and their performance is evaluated against the conventional Monte Carlo (MC) sampling using the Mersenne–Twister pseudorandom generator. The choice of the descent methods (steepest descent, Newton's and conjugate gradient methods), stabilizing functional (Tikhonov) and the regularization parameter (α) for gradient optimization were also examined. Gradient descent methods are an attractive choice for the current problem as analytical expressions for the Frechet and Hessian can be pre-computed for the Gaussian plume equation. For the current inverse problem, Newton's method with adaptive regularization and quadratic line-search is implemented. Since the forward modelling and measurement errors for atmospheric inverse problems are usually unknown, issues concerning 'model-fit' and 'data-fit' are examined.

As has been the central theme of this discussion, the area of application of inversion techniques to atmospheric source characterization problems is in its nascency and various methods are being tested and their performance is being evaluated. In the work presented in this article, a solution procedure different from the ones published in the literature is outlined. As with most of the other inversion techniques, the speed and accuracy of the present solution methodology depends on the noise level (δ) in the observed data (d_{obs}) and the quality of the forward model (A). When properly formulated, the solution to an inverse problem can help identify the necessary physics that need to be incorporated into A. Thus, inverse problems can in-turn be used to improve the speed and accuracy of the solution to the forward problem by enhancing or pruning the physics in the forward model.

2. Problem definition

In this section, the atmospheric inverse-source problem is defined mathematically.

Downloaded by [University of Utah], [Michael Zhdanov] at 13:16 07 October 2011

Downloaded by [University of Utah], [Michael Zhdanov] at 13:16 07 October 2011

2.1. *The forward problem*

The GPM is the simplest model that describes the dispersion of atmospheric contaminants. It is an analytical solution to the simplified advection–diffusion equation [19,23,24]. Of all the models used to characterize atmospheric dispersion, the GPM has the least computational complexity (requires minimum number of arithmetic operations). In emergency-response situations, the two most important factors are the speed and accuracy of reconstruction. The accuracy of reconstruction depends as much on the forward model (A) as it does on the inversion technique. Therefore, within its range of applicability, the GPM is the most desirable in such situations, due to the meagre cost associated with the forward model evaluation. Accordingly, the inverse-source problem is solved using the GPM for continuous point-releases as the forward operator. The GPM for steady, continuous and uniform wind conditions can be written as [23,24],

$$C_i(x_i, y_i, z_i) = \frac{Q_S}{2\pi u_S \sigma_y \sigma_z} \exp\left(\frac{-y^2}{2\sigma_y^2}\right)\left[\exp\left(\frac{-(z_i - z_S)^2}{2\sigma_z^2}\right) + \exp\left(\frac{-(z_i + z_S)^2}{2\sigma_z^2}\right)\right], \tag{2.1}$$

$$\sigma_y = \xi_1 x/\sqrt{1 + 0.0004x}, \quad \sigma_z = \xi_2 x, \tag{2.2}$$

$$x = -(y_R - y_S)\cos(\theta_S) - (x_R - x_S)\sin(\theta_S), \tag{2.3}$$

$$y = -(y_R - y_S)\sin(\theta_S) + (x_R - x_S)\cos(\theta_S). \tag{2.4}$$

Equation (2.1) gives an estimate of the concentration (C_i) at a receptor i with the position vector $\vec{X} = [(x_R - x_i), (y_R - y_i), (z_R - z_i)]$, where, x_S, y_S, z_S, and x_i, y_i, z_i, represent the source and the ith receptor spatial coordinates, respectively. The emission rate is Q_S, and the wind speed (u_S), and wind direction (θ_S) are assumed to be constant over the region of interest. The distances $(x_i - x_S)$, $(y_i - y_S)$, and $(z_i - z_S)$ are measured in the along-wind, cross-wind and vertical directions with the origin of the coordinate system being the source location. The parameters σ_y and σ_z (Equation (2.2)) are called the Gaussian plume spread parameters and account for the turbulent diffusion of the plume. They are empirical parameters and are defined for various meteorological stability conditions. For the present problem, Brigg's formulae for Pasquill C-type stability conditions were chosen [23,24]. These parameters, however are terrain and problem dependent and therefore for this work, the dimensionless empirical constants ξ_1 and ξ_2, which in Brigg's formulae are 0.22 and 0.20, were replaced by 0.12 and 0.10 for TCTE [15] as per the work of [9]. There are several other assumptions that are tacit in the Gaussian dispersion equation for which the reader may refer to [23,24].

It should be realized that the GPM is not a 'building-aware' model, in that it does not account for the changes in flow and dispersion patterns caused by buildings and other roughness elements when estimating the concentration value at a receptor in an urban domain. Therefore, depending on the terrain, the GPM may or may not be accurate in the near-field of a point source. In the far-field, since the plume is transported in the mesoscale wind direction, the constant wind direction assumption in the GPM becomes more admissible [25]. The solution methodology that will be developed in the subsequent sections is independent of the forward model used. The solution procedure developed can be applied with other versions of the GPM, or forward models that solve the governing equations for

fluid flow and dispersion [26]. It should however be noted that depending on the forward model used, the performance of the proposed solution procedure will vary.

The forward problem can be defined as estimating the concentrations at the desired receptor locations based on the given model (source) parameters (m) and can be written as

$$A(m) = d. \tag{2.5}$$

Here, A is the forward modelling operator (which in this case is the GPM), m is the set of model or source parameters and d is the vector of concentration measurements at the various receptor locations. For the computation of the concentration values at any point downwind of the source, the GPM requires eight model parameters (m_{GPM}). Hence, when using the GPM as the forward model, (2.5) can be written as

$$A(m_{\mathrm{GPM}}) = d, \tag{2.6}$$

$$m_{\mathrm{GPM}} = \begin{bmatrix} x_S & y_S & z_S & Q_S & u_S & \theta_S & \xi_1 & \xi_2 \end{bmatrix}^T_{8\times 1}, \tag{2.7}$$

$$d = \begin{bmatrix} d_1 & d_2 & \dots & d_N \end{bmatrix}^T_{N\times 1}. \tag{2.8}$$

2.2. *The inverse problem*

The inverse problem can be defined as the solution of the operator equation,

$$d = A(m). \tag{2.9}$$

The solution to the inverse problem requires determining such a model m_{pr} (predicted model) that generates predicted data, d_{pr}, which 'fits-well' the observed data d_{obs} [1]. If the forward operator is nonlinear, the solution to the inverse problem can only be found iteratively. Therefore, nonlinear inverse problems are often cast as minimization or optimization problems as shown below:

$$\arg\left(\min_{m_{\mathrm{pr}}} \left\| A(m_{\mathrm{pr}}) - d_{\mathrm{obs}} \right\|_2\right). \tag{2.10}$$

From (2.1) and (2.7), it can be deduced that when solving the source-inversion problem using the GPM, at most eight model parameters can be retrieved (m_{GPM}). Of these eight parameters, since the source strength (Q_S) and the wind velocity at the source (u_S) are a fraction of each other in the Gaussian equation (Equation (2.1)), attempting to retrieve them individually can result in non-unique solutions for these parameters. Therefore, they were combined into a single term (Q_S/u_S) in the present solution procedure.

The following five ($m_{\mathrm{STOCH+GD}}$) of the eight model parameters (m_{GPM}) (Equation (2.7)) in the GPM (Q_S and u_S combined into a single term (Q_S/u_S)) are retrieved in this work for TCTE:

$$m_{\mathrm{STOCH+GD}} = \begin{bmatrix} x_S & y_S & z_S & Q_S/u_S & \theta_S \end{bmatrix}^T_{5\times 1}. \tag{2.11}$$

Hence, the inverse-source problem is a five-dimensional (5D) inverse problem. The rationale behind retrieving five model parameters is based on the relationship between the increasing nonlinearity of inversion and the number of model parameters to be retrieved.

Downloaded by [University of Utah], [Michael Zhdanov] at 13:16 07 October 2011

Downloaded by [University of Utah], [Michael Zhdanov] at 13:16 07 October 2011

With the GPM, if only Q_S or u_S are to be retrieved, the inverse problem is in fact linear (Equation (2.1)). Nonlinearity creeps into the GPM from the remaining six model parameters. It is also well-accepted that an increase in the number of unknown model parameters leads to greater correlation between the model parameters, thereby resulting in non-unique solutions. The simple analytical nature of the Gaussian dispersion equation therefore raises the important question of the number of model parameters that one would want to retrieve (ideally eight) versus the accuracy of inversion. Non-uniqueness in inverse problems may be mitigated by including any prior information (m_{apr}) about the parameter values. But including prior information can compromise the robustness of the inversion technique as it can be inaccurate for a certain source release scenario. Hence, when using a simple analytic forward model such as the GPM for inversion, the question of number of retrievable model parameters should be addressed *a priori*. Therefore, in this work, five model parameters are retrieved (Equation (2.11)). The stochastic search stage is implemented with broad bounds on the model parameter values and unconstrained gradient optimization is performed with the initial iterate provided by the stochastic search stage.

3. The Copenhagen tracer experiments

In this work, data from the Copenhagen field experiments [15] is used to explain and validate the proposed solution procedure. The dataset used from the Copenhagen experiments is briefly described in this section.

As part of the Copenhagen experiment, the tracer sulphurhexafluoride (SF_6) was released without buoyancy from a tower of height 115 m. It was collected 2–3 m above the ground-level by sensors placed in three crosswind arcs positioned 2–6 km from the point of release. The first (Arc 1), second (Arc 2) and third (Arc 3) arcs were at radial distances of 2, 4 and 6 km from the source. The receptor locations and the source release location are shown in Figure 1. A total of 40 tracer-samplers were used with 15 sensors placed in Arc 1, 12 in Arc 2 and 13 in Arc 3. Three consecutive 20-min averaged tracer concentrations were measured, allowing for a total sampling time of 1 h. The site was mainly residential having a roughness length (z_0) of 0.6 m. The experiments were conducted on different days under neutral and unstable meteorological stability conditions. For this work, the experiment conducted on 19 October 1978/1979 is considered. The experiment was conducted mid-day, thereby resulting in unstable meteorological conditions (Monin–Obukhov length $L \sim -108$ m, friction velocity $u_* \sim 0.39\,\text{m s}^{-1}$, inversion height ~ 1120 m, standard deviation of the lateral and vertical velocities at the release point $\sigma_v \sim 0.85\,\text{m s}^{-1}$ and $\sigma_w \sim 0.68\,\text{m s}^{-1}$, stability class = Pasquill C-type) The emission rate was $3.2\,\text{g s}^{-1}$ and the limit of estimation (LOE) of the sensors was $9\,\text{ng m}^{-3}$. In the Copenhagen dataset [15], the mean value of the three consecutive 20-min averaged concentration datasets for the experiment conducted on 19 October is provided. In this work, this dataset is used as the observed data for inversion. The minimum positive concentration in the observed data vector from TCTE is $6\,\text{ng m}^{-3}$. Therefore for inversion, the value of LOE is set to $6\,\text{ng m}^{-3}$ instead of $9\,\text{ng m}^{-3}$. The average temperature (t_S), wind speed (u_S) and direction (θ_S) at the release height during the course of the experiment were $t_S \sim 283.72$ K, $u_S \sim 4.92\,\text{m s}^{-1}$ and $\theta_S \sim 308.6^\circ$. For the validation of the proposed inversion technique, the height of the sensors is considered to be 2.5 m.

It is worth noting that for the 19 October experiment, 34 out of the 40 sensors recorded positive concentrations (received a hit). These have been denoted by the 'squares' (□)

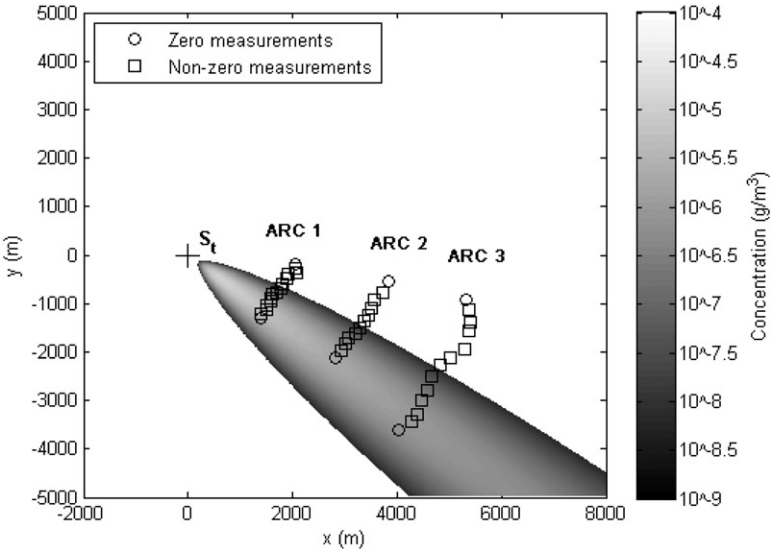

Figure 1. Schematic depicting the sensor positioning and the number of non-zero (□) and zero (○) measurements recorded for TCTE on 19 October. Also shown is the plume spread predicted by the GPM for true source parameters (m_t). 'S_t' is the true source location.

in Figure 1. As stated in Section 1, the total error that needs to be accounted for during the estimation stage is the sum of the following individual error components:

$$\text{Estimation error } (\delta_E) = \text{forward modelling error } (\delta_{\mathrm{FM}}) + \text{measurement error } (\delta_{\mathrm{M}}). \tag{3.1}$$

Since the authors of the report [15] make no mention of the uncertainties in the measurements, δ_{M} is assumed to be zero (i.e. $\delta_{\mathrm{E}} = \delta_{\mathrm{FM}}$). The rationale behind setting $\delta_{\mathrm{M}} = 0$ lies in the definition of the LOE in atmospheric source-inversion problems. For instance, assuming 5% noise in the observed data can result in certain non-zero measurements going below the LOE, thereby becoming zero. Since the locations of zero and non-zero measurements are of paramount importance for source characterization, the measurements were not tampered with by assuming noise levels. In order to get a feel for δ_{FM} when using the GPM, the forward problem was solved with the known source parameters, with $\xi_1 \approx 0.12$ and $\xi_2 \approx 0.1$ (from the work of [9]). The results obtained are shown in Figure 1. From the figure it is evident that despite using the modified σ_y and σ_z values, the plume spread predicted by the GPM does not match the experimental measurements.

The difference in the plume spread predicted by the GPM can be attributed to the complexities associated with real-world flows that are incorporated into the present version of the GPM. Since $\delta_{\mathrm{E}} = \delta_{\mathrm{FM}}$, and δ_{FM} is due to the inadequacies of the forward model and cannot be quantified, the inversion procedure developed (and described in subsequent sections) is designed to drive the forward model to match the zero and non-zero measurements recorded by the sensors. That is, the inversion procedure developed ensures that at the end of inversion, the plume spread predicted by the GPM is as close as possible to that observed in the experiments, not in terms of magnitudes of

Downloaded by [University of Utah], [Michael Zhdanov] at 13:16 07 October 2011

concentration measurements, but in terms of the zero and non-zero measurements recorded by the respective sensors.

Definition 1 Whenever the predicted model parameters generate non-zero ($\geq$LOE) predicted data at a receptor that recorded a non-zero concentration ($\geq$LOE), or zero ($<$LOE) predicted data at a receptor that recorded a zero concentration value ($<$LOE), it will from hereon be said that the predicted model parameters 'satisfy' the concentration measurement at the receptor location.

The true model parameters (m_t) for TCTE are shown in Equation (3.2). The bounds of the model parameter space considered during inversion are shown in Equation (3.3).

$$\begin{aligned} m_t &= \begin{bmatrix} x_S(m) & y_S(m) & z_S(m) & Q_S/u_S(g/m) & \theta_S(^\circ) \end{bmatrix}_{5\times1}^T \\ &= \begin{bmatrix} 0 & 0 & 115 & 0.65 & 308.6 \end{bmatrix}_{5\times1}^T, \end{aligned} \tag{3.2}$$

$$x_S \in [-2000, 8000], \quad y_S \in [-5000, 5000], \quad z_S \in [0, 200], \quad Q_S/u_S \in [0, 1], \quad \theta_S \in [0, 360]. \tag{3.3}$$

4. Solution procedure

4.1. *The Tikhonov parametric functional*

In this work, the atmospheric inverse-source problem is solved using a combination of stochastic search and regularized gradient optimization methods. Regularization provides a mechanism by which any prior information can be included in the inversion procedure. Including prior information can help improve the stability of inversion. The regularized solution of an inverse problem can be obtained by minimizing the unconstrained parametric functional shown in Equation (4.1).

$$P(m, d, \alpha) = \mu_D(A(m), d) + \alpha s(m), \tag{4.1}$$

$$\arg\left(\min_m P(m, d, \alpha)\right). \tag{4.2}$$

In Equation (4.1), $\mu_D(A(m), d)$ is the misfit functional (over the data space (D)), $s(m)$ is the stabilizing functional and $P(m, d, \alpha)$ is the parametric functional. The parametric functional is a linear combination of the misfit and the stabilizing functionals, and the parameter α is called the regularization parameter.

The role of the misfit functional is to check if, on every step of inversion, the discrepancy between the observed and the predicted data is increasing or decreasing. Since most real-life inverse problems are ill-posed, casting the inverse problem as the minimization of the misfit functional can result in unstable solutions. This is because the operator A^{-1} may not be continuous (may not exist) over the entire model space (M). The inherent ill-posedness of inverse problems can be overcome by considering a family of well-posed problems ($d = A_\alpha(m)$) that approximate the original ill-posed problem ($d = A(m)$). The scalar parameter $\alpha > 0$ in the above expression is called the regularization parameter and regularization is imposed under the constraint $m_\alpha \to m_T$; as $\alpha \to 0$

Downloaded by [University of Utah], [Michael Zhdanov] at 13:16 07 October 2011

(where m_T is the true solution). That is, regularization approximates the non-continuous operator A^{-1} by the family of continuous operators $A_\alpha^{-1}(d)$ for different values of α. The family of continuous $A_\alpha^{-1}(d)$ operators that approximate the original non-continuous operator A^{-1} are called the regularization operators $R_\alpha(R(d,\alpha) = A_\alpha^{-1}(d))$. Regularization operators can be constructed by adding a stabilizing functional to the misfit functional. The task of the stabilizing functional is to help identify from the set of all possible models that fit the data, a solution that belongs to the correctness-set $M_C(M_C \subset M)$, such that the operator A^{-1} is continuous over M_C. Formulating an inverse problem in this manner converts an ill-posed problem into a 'conditionally well-posed problem', expressed by the parametric functional in Equation (4.1)

In this article, Equation (4.1) is minimized using Newton's method. Gradient methods require the misfit functional to be convex, continuous and differentiable (C-C-D) to converge to the global minimum. Examining the GPM, one can recognize that the misfit functional generated by the GPM (using Equation (4.4)) has multiple critical points (maxima, minima and saddle points). In fact, when using the GPM, the number of maxima in the misfit functional space is a function of the domain size, the wind direction at the source (θ_S) and the number of sensors (N) in the domain. This can be shown by considering the GPM in Equation (2.1). For instance, if in Equations (2.1)–(2.4), $x_S = x_i$, $y_S = y_i$, and $z_S = z_i$, then, in (2.1),$C_i(x_i, y_i, z_i) = NaN(= 0/0)$. If x_i, y_i and z_i, approach x_S, y_S and z_S at the same rate, for some fixed θ_S, the predicted concentration in (2.1) approaches infinity.

Thus, it is seen that when using the GPM, whenever the predicted source location is close to any of the receptor locations, there is an increase in the misfit functional value. The presence of the various maxima in addition to the various error components (δ_{E} and δ_{A}) results in the formation of several critical points interspersed around the global minimum. Therefore, to employ gradient schemes to solve such problems, a good starting solution is pivotal. The starting solution needs to be in the C-C-D region surrounding the global minimum in the misfit functional space. For this reason, the approach proposed in this article is comprised of stochastic search to provide a good initial iterate to the gradient descent scheme (that may be in the C-C-D region).

In order to illustrate that the proposed approach works for inverse-source problems with the GPM as the forward operator, the domain of TCTE (Figure 1) was discretized and the misfit functional at every grid node was computed using Equation (4.4). This was done in two-dimensions (2D) by considering the x and y coordinates of the source (x_S and y_S) to be the unknown model parameters (m). The results obtained are shown in Figure 2(a) and (b). From the figures it can be seen that as $x_S \to x_i$ and $y_S \to y_i$, $\left|(d_{\mathrm{obs}})_i - \left(d_{\mathrm{pr}}\right)_i\right| \uparrow$ (*increases*). This behaviour is in agreement with the previously stated assertion that as $x_S \to x_i$ and $y_S \to y_i$, $C_i(x_i, y_i, z_i) = \left(d_{\mathrm{pr}}\right)_i \to \infty$. From the figures it can also be deduced that there exists a region in the misfit functional space in which the misfit functional appears to be convex and continuous, and houses the global minimum. The plots also shed light on the distortion of the misfit functional by the forward modelling error δ_{FM} (assuming $\delta_{\mathrm{M}} = 0$). The distortion manifests itself in terms of the discrepancy observed in the predicted S_p (square – ■) and the true source locations S_t (hexagon – ✸) as shown in Figure 2(b). However, not too many conclusions should be drawn from these plots as they are in 2D. In 5D, the hyper-volume that spans the C-C-D region might be of different size and corrugated, due to the effects of nonlinear error propagation.

Downloaded by [University of Utah], [Michael Zhdanov] at 13:16 07 October 2011

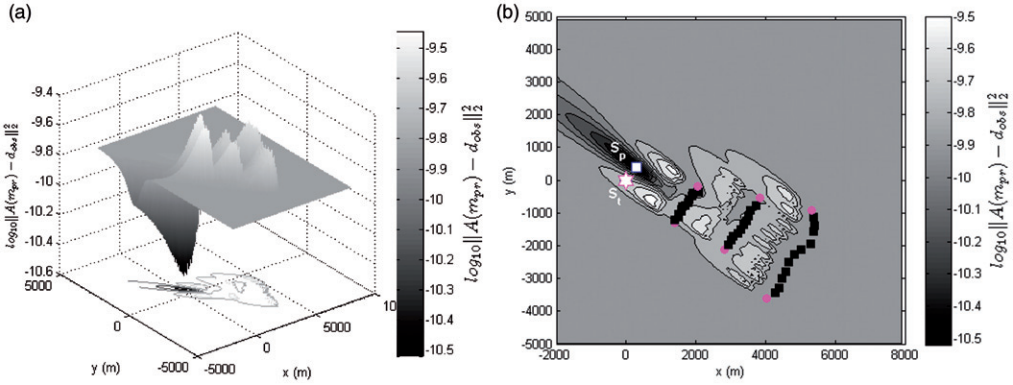

Figure 2. (a) Surface of the misfit functional for TCTE, (b) 2D contour of the misfit functional for TCTE data with the true (S_t) and predicted (S_p) source locations.

4.2. *The misfit functional*

The definition of the misfit functional is one of the most important components of an inverse problem. When properly formulated, it guides the inversion algorithm to the global minimum. Misfit functional formulation, just like the choice of an inversion algorithm, is highly problem dependent. Some of the popular formulations of misfit functionals are based on the L_1- and L_2-norms of the misfit (Equations (4.3) and (4.4)), the L_1- and L_2-norms of the relative misfit, the Kullback–Leibler information divergence functional (Equation (4.5)) and the negative Poisson log-likelihood functional (Equation (4.6)) [27,28].

$$\mu_{L_1}\big(A(m_{\mathrm{pr}}), d_{\mathrm{obs}}\big) = \big\|A(m_{\mathrm{pr}}) - d_{\mathrm{obs}}\big\|_1, \tag{4.3}$$

$$\mu_{L_2}\big(A(m_{\mathrm{pr}}), d_{\mathrm{obs}}\big) = \big\|A(m_{\mathrm{pr}}) - d_{\mathrm{obs}}\big\|_2, \tag{4.4}$$

$$\mu_{\mathrm{KL}}\big(A(m_{\mathrm{pr}}), d_{\mathrm{obs}}\big) = \big\langle A(m_{\mathrm{pr}}), \log\big(A(m_{\mathrm{pr}})/d_{\mathrm{obs}}\big)\big\rangle, \tag{4.5}$$

$$\mu_{\mathrm{LHD}}\big(A(m_{\mathrm{pr}}), d_{\mathrm{obs}}\big) = \big\langle A(m_{\mathrm{pr}}), 1\big\rangle - \big\langle d_{\mathrm{obs}}, \log\big(A(m_{\mathrm{pr}})\big)\big\rangle. \tag{4.6}$$

Computing the L_2-norm or the L_1-norm of the misfit to determine the class of models (m_{pr}) that fit the observed data (d_{obs}) can lead to erroneous results for the atmospheric source-inversion problem. This is primarily because atmospheric inverse-source problems suffer from sparse number of measurements (N) in general, and very few non-zero measurements (N_{NZ}) in particular. Therefore, computation of the L_1-or L_2-norms (Equations (4.3) and (4.4)) does not take into account the zero-measurements recorded by the sensors, as the magnitude of these norms are driven only by the non-zero measurements. Also, since the observed and predicted data vectors in atmospheric inverse-source problems consist of concentration values of varying orders of magnitudes, the larger components of the observed and predicted data vectors suppress the effect of the smaller components in the computed value of the norm of the residuals.

Downloaded by [University of Utah], [Michael Zhdanov] at 13:16 07 October 2011

To mitigate the above-mentioned problems, one can use an appropriate data-weighting matrix such that the significance of the individual components of the predicted and observed data vectors is preserved during inversion. In this article, an even simpler approach (misfit functional) is proposed and is described in the following paragraphs.

Our new misfit functional takes into account zero and non-zero measurements in the observed and predicted data vectors and treats both of them equally. The new functional uses the base 10 logarithm of the ratio of the observed (d_{obs}) and predicted data (d_{pr}), and is shown in Equation (4.7). In Equation (4.7), $I\{\}$ is the indicator function, and is defined in Equation (4.8). The positive constant ε ($\varepsilon \ll$ LOE) accounts for the zero measurements and becomes insignificant for non-zero measurements. For the present work, ε value was set to 10^{-16}.

$$\mu_D(d_{\mathrm{obs}}, d_{\mathrm{pr}}) = \left(\sum_{i=1}^{N} I\left\{ \left(\log_{10}\left[\frac{(d_{\mathrm{obs}})_i + \varepsilon}{(d_{\mathrm{pr}})_i + \varepsilon} \right] \right) \in \Omega \right\} \right)^{-1}, \tag{4.7}$$

$$\Omega = [\beta_{\mathrm{LB-STOCH}}, \beta_{\mathrm{UB-STOCH}}]$$
$$I_\Omega(x) = \begin{cases} 1, & \text{if } x \in \Omega, \\ 0, & \text{if } x \notin \Omega. \end{cases} \tag{4.8}$$

The applicability of the proposed misfit functional is based on the fact that for inversion without noise, the end result of inversion should give predicted model parameters (m_{pr}), such that for $m_{\mathrm{pr}} \approx m_{\mathrm{t}}$, $((d_{\mathrm{obs}})_i + \varepsilon)/((d_{\mathrm{pr}})_i + 1) \approx 1$, $\forall i$. The bounds $\beta_{\mathrm{LB-STOCH}}$ and $\beta_{\mathrm{UB-STOCH}}$ are the lower and upper bounds (data-fit criteria) of the stochastic search stage and depend upon the noise level (δ_{M}) in the observed data (d_{obs}), the forward modelling error (δ_{FM}) and the accuracy to which one wants to implement the search stage. Depending on the values of $\beta_{\mathrm{LB-STOCH}}$ and $\beta_{\mathrm{UB-STOCH}}$, the search stage can either be computationally exorbitant or inexpensive. Strategies to solve the inverse-source problem in general, and to compute the bounds $\beta_{\mathrm{LB-STOCH}}$ and $\beta_{\mathrm{UB-STOCH}}$ in particular are described in the subsequent sections.

The new misfit functional is used in the stochastic search stage to identify a good starting solution for the gradient descent scheme. It should be noted that the starting solution (m_{STOCH}) is a function of the values of $\beta_{\mathrm{LB-STOCH}}$ and $\beta_{\mathrm{UB-STOCH}}$, and the values of $\beta_{\mathrm{LB-STOCH}}$ and $\beta_{\mathrm{UB-STOCH}}$ characterize the size of the hyper-volume constituting the C-C-D region (based on L_2-norm) around the global minimum in the misfit functional space. Due to this, care should be taken in the selection of $\beta_{\mathrm{LB-STOCH}}$ and $\beta_{\mathrm{UB-STOCH}}$ values, since large values of these parameters may no longer provide an initial iterate (m_{STOCH}) in the C-C-D region surrounding the global minimum for problems with misfit functional spaces comprising several critical points. Since gradient methods only work with continuous and differentiable misfit functionals, the conventional misfit functional based on L_2-norm (Equation (4.4)) is used for computing the new iterates for the gradient scheme.

4.3. *Strategies for solving the atmospheric source-inversion problem*

In this section, strategies for solving the atmospheric source characterization problem in general and computing the bounds $\beta_{\mathrm{LB-STOCH}}$ and $\beta_{\mathrm{UB-STOCH}}$ in particular are discussed.

Downloaded by [University of Utah], [Michael Zhdanov] at 13:16 07 October 2011

Downloaded by [University of Utah], [Michael Zhdanov] at 13:16 07 October 2011

Three strategies are proposed to solve the inverse-source problem. They are described in the following sections:

4.3.1. *Rigorous strategy*

The objective of this strategy is to 'satisfy' (Definition 1) all the sensor measurements (N). This is the preferred strategy for evaluating atmospheric dispersion models (forward models) using field experiment data. The same approach can be adopted to solve inverse-source problems using the forward model (dispersion model). In spite of being the most rigorous method to solve such problems, this approach cannot be implemented for all real-life atmospheric dispersion situations and for increasing number of sensor measurements (N). This is because, the effects of myriads of real-world processes are not captured in totality by the existing forward dispersion models (A) in general, and the GPM in particular. Since in this article, field experiment data (TCTE) are used to retrieve the model parameters ($m_{\mathrm{STOCH+GD}}$), the rigorous strategy is not adopted. However, 10^8 MC simulations (points) with the semi-rigorous strategy described in Section 4.3.2.1 and with $\beta_{\mathrm{LB-STOCH}}$ and $\beta_{\mathrm{UB-STOCH}}$ values prescribed in Section 4.4 were run to illustrate that in spite of running an astronomical number of MC simulations, all the sensor measurements for TCTE cannot be satisfied. For the final model parameters obtained (m_{STOCH}), the maximum number of sensor measurements ($N_{\mathrm{max-S}}$) satisfied were 39 out of the available 40 measurements, and out of the 10^8 random samples (model parameter vectors) only four model parameters satisfied 39 measurements.

4.3.2. *Semi-rigorous strategy*

The objective of this strategy is to satisfy most, but not all the sensor measurements (N). The number of sensor measurements that should be satisfied (N_{S}), or the percentage of the total number of measurements (N) that should be satisfied ($\lambda_N = 100 \times N_{\mathrm{S}}/N$) for the predicted solution to be in the vicinity of the true solution is problem-specific, and depends upon the number of available sensor measurements (N), the number of model parameters to be retrieved (N_{m}), and the quality of the forward model (A). While λ_N values close to 100% make the stochastic search stage computationally intensive, relaxed values of λ_N might produce initial iterates that do not belong to the C-C-D region surrounding the global minimum.

It should be noted that while solving inverse-source problems, fixing values of N_{S} might result in erroneous source locations. This is because the inversion algorithm might end up not accounting for either only the zero or non-zero measurements to satisfy the λ_{N} value assigned. To avoid such pitfalls, if N_{NZ} and N_{Z} represent the number of zero and non-zero measurements recorded ($N_{\mathrm{NZ}} + N_{\mathrm{Z}} = N$), it is suggested that N_{S} should be divided into its individual components based on the number of zero ($N_{\mathrm{S-Z}}$) and non-zero ($N_{\mathrm{S-NZ}}$) measurements ($N_{\mathrm{S}} = N_{\mathrm{S-Z}} + N_{\mathrm{S-NZ}}$) that should be satisfied. Assigning λ_N values based on the percentage of zero ($\lambda_Z = 100 \times N_{\mathrm{S-Z}}/N_{\mathrm{Z}}$) and non-zero ($\lambda_{\mathrm{NZ}} = 100 \times N_{\mathrm{S-NZ}}/N_{\mathrm{NZ}}$) measurements should (will) improve the accuracy of the inverse problem solution. Based on how the λ_N values are determined, the semi-rigorous strategy can be implemented in three ways, which are as given in the following sections.

4.3.2.1 *Semi-rigorous strategy 1 (SR1)*. SR1 comprises satisfying λ_{N} measurements without assigning individual values for λ_{NZ} and λ_{Z}. It is the least robust of all the

semi-rigorous strategies and produces initial iterates in the C-C-D region only for large values of λ_N. To get an idea about the minimum λ_N value for the TCTE that makes the solution procedure fail-safe, the MC simulations used to compute N_{max-S} were utilized. From the simulations it was deduced that for making the stochastic search stage fail-safe (i.e. generate initial iterates in the C-C-D region), at least 37 sensors (92.5% of the observed data) had to be satisfied. To evaluate the performance of the various QMC point-sets, the number of MC and QMC points required for satisfying $N_S = 37$, 38 and, 39 sensors are compared in this article (discussed in section 5.2).

4.3.2.2 *Semi-rigorous strategy 2 (SR2)*. SR2 comprises assigning individual values for λ_{NZ} and λ_Z. For the TCTE, based on the 10^8 MC simulations, the following details were observed: (1) if all the zero measurements are satisfied ($N_{S-Z} = 6$), the minimum number of non-zero measurements that need to be satisfied to make the solution procedure fail-safe is $N_{S-NZ} \geq 27$, (2) if $N_{S-Z} = 5$, then $N_{S-NZ} \geq 31$ and (3) for $1 \leq N_{S-Z} \leq 4$, $N_{S-NZ} \geq 33$. These details are illustrated in Figure 3. The benefit of assigning individual values for λ_{NZ} and λ_Z is that the value of N_S required for identification of an initial iterate can be brought down. That is, if all six zero measurements are satisfied, then the minimum number of non-zero measurements that need to be satisfied is 27, which makes $N_S \geq 33$ ($N_S \geq 37$ for SR1 for the solution procedure to be fail-safe). In this article, for conciseness, the results for SR2 are not presented.

4.3.2.3 *Semi-rigorous strategy 3 (SR3)*. In SR3, all non-zero measurements must be satisfied. The number of zero measurements that should be satisfied is problem dependent. The rationale behind setting $\lambda_{NZ} = 100\%$ is based on the idea that over-prediction is always better than under-prediction. Setting $\lambda_{NZ} = 100\%$ and $\lambda_Z \leq 100\%$ implies over-predicting the extent of the plume spread, which implies over-predicting the

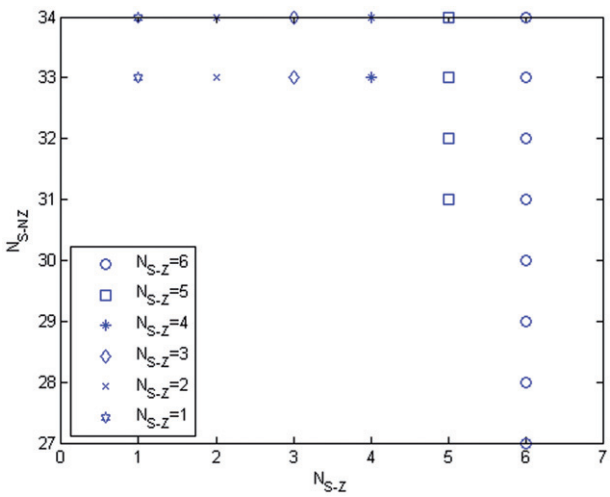

Figure 3. The number of zero (N_{S-Z}) and non-zero (N_{S-NZ}) measurements that should be satisfied to obtain initial iterates in the C-C-D region for TCTE. The details of this figure are highly problem-dependent. They also depend on the plume spread parameters chosen.

Downloaded by [University of Utah], [Michael Zhdanov] at 13:16 07 October 2011

source strength. This is the preferred approach in atmospheric dispersion problems as over-prediction implies a higher factor of safety. For evaluating the performance of the various QMC point-sets, results for the cases when $N_{S-Z} \geq 1$, 2, 3, 4 and 5 are reported (in Section 5.2).

4.4. *Computing the bounds $\beta_{LB-STOCH}$ and $\beta_{UB-STOCH}$*

The two scenarios that should be avoided when solving the inverse-source problem are:

(1) predicting non-zero concentrations at sensors that recorded zero measurements, and
(2) predicting zero concentrations at non-zero sensor locations. Whenever these scenarios occur, the stochastic search algorithm must be able to identify them and reject the generated (predicted) model parameters (m_{pr}). The two scenarios mentioned help compute the bounds for the stochastic search stage. The method for computing the bounds is described below.

Case 1

$$(d_{obs})_i = 0, \quad \left(A(m_{pr})\right)_i \neq 0$$

At a sensor location where the observed data is zero (<6 ng), the predicted data can take either a zero (<6 ng) or a non-zero value (≥6 ng). The smallest non-zero value that $\left(d_{pr}\right)_i$ can take so that the definition of LOE is preserved is 6×10^{-9}g (= LOE (=6 ng)). From this, $\beta_{LB-STOCH}$ can be estimated as

$$\beta_{LB-STOCH} \approx \log_{10}[\varepsilon/\text{LOE}] \approx \log_{10}\left[10^{-16}/6 \times 10^{-9}\right] \approx -7.78. \tag{4.9}$$

Case 2

$$(d_{obs})_i \neq 0, \quad \left(A(m_{pr})\right)_i = 0$$

Predicted data values of zero can occur at receptor locations with non-zero measured values. If zero concentration is predicted at the receptor that recorded the maximum concentration, it is more likely that the predicted model parameters (m_{pr}) that generated the predicted data (d_{pr}) are incorrect. The likelihood of the predicted model parameters being close to the true model parameter is higher if $\left(d_{pr}\right)_i = 0$ occurs at the receptor that recorded the minimum concentration value. Since the noise level in the data in unknown, the smallest non-zero value that the observed data vector (d_{obs}) can take is 6 ng. Hence, $\beta_{UB-STOCH}$ can be estimated as

$$\beta_{UB-STOCH} \approx \log_{10}[\text{LOE}/\varepsilon] \approx \log_{10}\left[6 \times 10^{-9}/10^{-16}\right] \approx 7.78. \tag{4.10}$$

Based on the values of $\beta_{LB-STOCH}$ and $\beta_{UB-STOCH}$ derived, it can be seen that the semi-rigorous strategy allows for considerable over- and under-prediction of the concentrations at the receptors.

4.5. *MC and QMC sampling*

QMC point-sets and MC sampling are considered in the stochastic search stage. QMC sampling is recommended over the conventional MC sampling as quasi-random numbers

Downloaded by [University of Utah], [Michael Zhdanov] at 13:16 07 October 2011

were developed to fill an s-dimensional hyper-cube on $[0,1)^s$ more uniformly than pseudorandom numbers [29]. Additionally, QMC point-sets provide the extra advantage of being completely deterministic. This property of QMC point-sets is highly desirable for atmospheric event reconstruction problems. This is because, for known receptor locations, stochastic algorithms developed to solve the inverse-source problem for a real city can be tested for a large set of possible model parameter values, and the performance of the algorithm in terms of total execution time (which is equivalent to the number of forward model evaluations) can be determined *a priori*.

QMC sampling is performed using the Halton, Hammersley, Sobol, SpecialNeiderreiter and NeiderreiterXing point-sets [29,30], in their original and scrambled forms. The scrambled versions of the Halton, Hammersley, SpecialNeiderreiter, and NeiderreiterXing point-sets were obtained by applying Faure permutations over the original set [29]. The scrambled version of the Sobol point-set was obtained by applying the scrambling procedure described in [31], a random linear scramble combined with a random digital shift.

For comparing the performance of the various QMC point-sets with the Mersenne–Twister pseudorandom generator, the expected number of MC points $E(\mathrm{MC})$ required for satisfying a given set of sensor measurements were used. The quantity $E(\mathrm{MC})$ was computed from the 10^8 MC simulations run to compute $N_{\max-\mathrm{S}}$. Leaving the Hammersley point-set, the ith components of all other QMC point-sets considered are independent of the number of points generated (n: $n \geq i$). This is because, only in the Hammersley point-set, the first dimension is a regular one-dimensional (1D) lattice evenly distributed on the interval $[0,1)$. Therefore for accurate comparison of the performance of the Hammersley point-set with the pseudorandom generator, $E(\mathrm{MC})$ number of Hammersley points were generated to satisfy $N_{\mathrm{S}} = k$ measurements.

4.6. *The stabilizing functional, regularization parameter and gradient methods*

The stabilizing functional $s(m)$ in conjunction with the regularization parameter α is used to construct the regularization operator R_α that converts an ill-posed problem into a 'conditionally-well-posed' problem (Equation (4.1)). For the inverse-source problem, the standard Tikhonov stabilizing functional was chosen as the stabilizing functional. The Tikhonov stabilizer is shown in Equation (4.11). The vector m_{apr} represents some prior information that we might have about the model parameters (m). No prior information was assumed in the solution procedure for the atmospheric event reconstruction problem. However, a modified version of the stabilizer shown in Equation (4.11) was used in the descent algorithm and is shown in Equation (4.12). The rationale behind using this stabilizer is based on the initial iterate provided by the stochastic search stage. The stochastic search stage was designed to provide a starting solution that belongs to the C-C-D hyper-volume around the global minimum. Therefore, to ensure that the gradient scheme does not bounce out of the C-C-D region, the model parameters on the current (j) and previous iterations ($j-1$) were used to stabilize the gradient scheme.

$$s(m) = \left\| m - m_{\mathrm{apr}} \right\|_2^2, \tag{4.11}$$

$$s(m) = \left\| m^j - m^{j-1} \right\|_2^2, \quad j = 2, 3, \ldots. \tag{4.12}$$

Downloaded by [University of Utah], [Michael Zhdanov] at 13:16 07 October 2011

Downloaded by [University of Utah], [Michael Zhdanov] at 13:16 07 October 2011

The regularization parameter α determines the relative significance of the misfit and the stabilizing functionals. Choosing extremely small values of α leads to the situation where the inverse problem reduces to the minimization of the misfit functional, which can result in unstable solutions. Large values of α correspond to the situation where the inverse problem is driven in the direction of the stabilizer. Hence, accurate reconstruction requires optimal regularization parameter selection. Several methods have been proposed for optimal regularization parameter selection. Prominent among these are the Morozov condition [28] and the L-curve criterion [1,27,28,32]. In this article, a more heuristic approach as suggested in [1] was adopted. The regularization parameter was estimated following Equations (4.13) and (4.14). The first iteration of the gradient scheme is run without regularization and α^1 is calculated at the end of the iteration following Equation (4.13). Values of α on the subsequent iterations are computed using (4.13). In Equation (4.14), the scalar q helps control the extent of regularization. Lower values of q favour faster convergence, but can lead to instabilities in the inversion procedure. Higher values of q promote better stability, but result in more iterations for convergence. In this work, the initial value of q was set to 0.7 and was decreased by raising it to the power of the previous iteration number $(j-1)$ as shown in Equation (4.14).

$$\alpha^1 = \left\| A(m^1) - d_{\text{obs}} \right\|_2^2 / \left\| m^1 - m^0 \right\|_2^2, \tag{4.13}$$

$$\alpha^j = \alpha^1 q^{j-1}, \quad (0 < q < 1), \quad j = 2, 3, \ldots. \tag{4.14}$$

Following Equations (4.4) and (4.12)–(4.14), the unconstrained parametric functional described in Equation (4.1) can be written as

$$P^j\left(m^j, d_{\text{obs}}, \alpha^j\right) = \left\| A\left(m^j\right) - d_{\text{obs}} \right\|_2^2 + \alpha^j \left\| m^j - m^{j-1} \right\|_2^2. \tag{4.15}$$

The parametric functional shown in Equation (4.15) is minimized using Newton's method. To ensure convergence and to prevent overshooting of the Newton jump, quadratic line-search was implemented. For computational efficiency, the Hessian is approximated by calculating the residual assuming unit-step with linear line-search. Additional details of the algorithm implemented can be found in [1].

4.7. *The hybrid algorithm conundrum*

Hybrid algorithms are an attractive choice for solving optimization problems as they can help increase the speed of convergence of the algorithm. It is for this reason that they have been used extensively in several problems from diverse fields and also in problems involving atmospheric source characterization [18,20,33]. The solution procedure described in this article is also a hybrid approach comprising stochastic search and gradient optimization, with different misfit functionals implemented in each stage. The stochastic search stage can be regarded as a crude maximization stage (because the likelihood of the initial iterate being close to the true source parameters increases with increasing N_S values), and the gradient descent stage can be regarded as the minimization stage (the residual of the observed and predicted data is minimized). The predicament arises when model parameters that maximize the number of sensors satisfied are different from model parameters that minimize the residual. This situation arises in real-life problems as the estimation error (Equation (3.1)) that needs to be accounted for is unknown. If the stochastic search stage is implemented with tight error bounds

Table 2. Computed inversion model parameters for TCTE.

Model parameters	x_S (m)	y_S (m)	z_S (m)	Q_S/u_S (gm^{-1})	θ_S (degrees)	N_S
m_t	0	0	115	0.64	308.57	–
m_{STOCH}	−650.81	736.72	3.08	0.73	297.22	37
$m_{STOCH*max(Ns)}$	91.05	−21.44	85.97	0.86	294.63	39
$m_{STOCH+GD}$	−339.78	73.6	193.42	1.06	291.73	34

Downloaded by [University of Utah], [Michael Zhdanov] at 13:16 07 October 2011

(for safety), and if the model parameters obtained from this stage (m_{STOCH}) satisfy $N_{STOCH} \leq N$ sensors, and if the model parameters computed by the gradient scheme ($m_{STOCH+GD}$) (using m_{STOCH}) are closer to the true model parameters (m_t), but satisfy lesser number of sensor measurements ($N_{STOCH+GD}$) than N_{STOCH}, then the question of which model parameters to believe more emerges. That is, if $N_{STOCH+GD} < N_{STOCH}$, but $\|m_{STOCH+GD} - m_t\| < \|m_{STOCH} - m_t\|$, in a real-time situation, should one go with m_{STOCH} or $m_{STOCH+GD}$? When using field experiment data to evaluate hybrid algorithms, since m_t is known *a priori*, the decision is relatively easy to make. However, in real-time, where m_t is unknown, then the question becomes: should one choose the model parameters that give the best 'data-fit' or 'model-fit'? Therefore, in this article, when the Mersenne–Twister generator is used, model parameters that produce the maximum N_S value, as well as the minimum residual, are presented (Section 5.1, Table 2).

4.8. *Implementing the proposed approach*

Almost all algorithms developed to solve inverse problems either have tuning parameters or parameters that require a good initial value or distribution. The approach proposed in this article is no different in that it also requires the specification of the parameter (λ) for its successful implementation. It should be realized that one might get away by considering the misfit functional based on the L_2-norm in the stochastic stage for some source-receptor configurations, and hence circumvent the need for the specification of a λ value, making the solution procedure free of tuning parameters (the convergence criterion for the L_2-norm can be deduced from the available data). However, a new misfit functional, and thereby the λ value were introduced only to make the solution procedure fail-safe. Since the optimum λ value is never available in real-life situations, it is recommended that the proposed approach be implemented with large λ values (using SR1, SR2 or SR3), or, implemented multiple times starting with λ values of 90% (for SR1: $\lambda_N = 90\%$, for SR2: $\lambda_{NZ} = \lambda_Z = 90\%$, for SR3: $\lambda_{NZ} = 100\%$ and $\lambda_Z = 90\%$) and with increments that result in integer values of N_{S-NZ} and N_{S-Z}. When choosing the initial λ value of 90% option, it is advantageous to note that since QMC point-sets are deterministic, the entire simulation need not be re-run in case λ values need to be incremented. Instead, only the QMC points that succeed the points required for satisfying the previously rejected λ value can be used for satisfying the current λ value. Also, since atmospheric inverse-source problems always comprise sparse number of sensor measurements (N), the maximum number of times that the proposed approach needs to be run is theoretically N. To provide the reader an estimate for the values of N, currently, approximately 500 sensors have been placed in

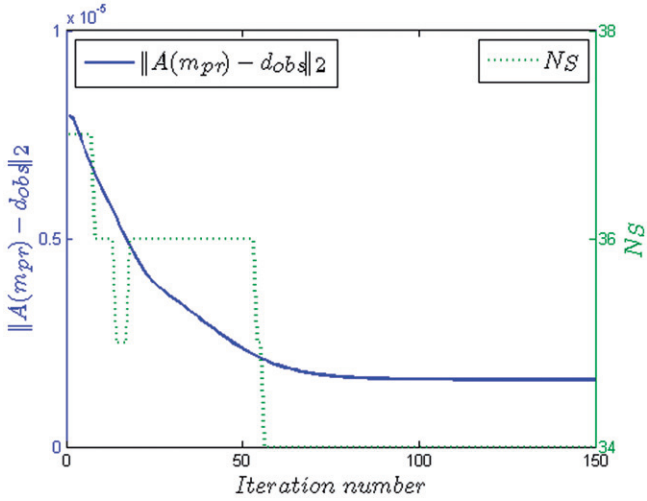

Figure 4. Convergence of Newton's method for TCTE.

31 US cities according to the Bio-Watch program, which on an average reduces to 16 sensors per city ($N = 16$) [34].

5. Results and discussion

5.1. *Final model parameters and comparison with results from the literature*

The final model parameters obtained using Newton's method are shown in Table 2. For these simulations, the Mersenne–Twister generator was used in the stochastic search stage (the random number seed was set equal to zero). In Table 2, m_t represents the true model parameters from TCTE. The parameters m_{STOCH} are the initial iterates obtained from the stochastic stage when SR1 was used with $N_S \geq 37$. The parameters $m_{\mathrm{STOCH*max}(N_S)}$ represent the model parameters that satisfy the maximum number of sensor measurements ($N_S = 39$). The final solution from Newton's method is denoted as $m_{\mathrm{STOCH+GD}}$. The convergence of Newton's method is illustrated in Figure 4. Based on the value of the norm of the residuals in the iteration space, as well several runs (using the Mersenne–Twister generator), it was found that when Newton's method converged, it converged at $N_S = 34$, after about 100 iterations (Figure 4). Irrespective of the strategy (SR1, SR2 or SR3) chosen to identify an initial iterate, Newton's method always converged to the final model parameters given by $m_{\mathrm{STOCH+GD}}$. This brings us to the question raised in Section 4.7 concerning 'model-fit' and 'data-fit'. From the results in Table 2 it can be clearly seen that the solution provided by Newton's method results in the minimum value of the norm of the residuals, while that provided by the stochastic search results in better 'data-fit'. The performance of the various QMC point-sets in terms of number of points required for identifying an initial iterate are discussed in the subsequent sections (Section 5.2). The performance of Newton's method in terms of number of iterations required to converge to the final solution depending on the strategy chosen is discussed in Section 5.3.

Downloaded by [University of Utah], [Michael Zhdanov] at 13:16 07 October 2011

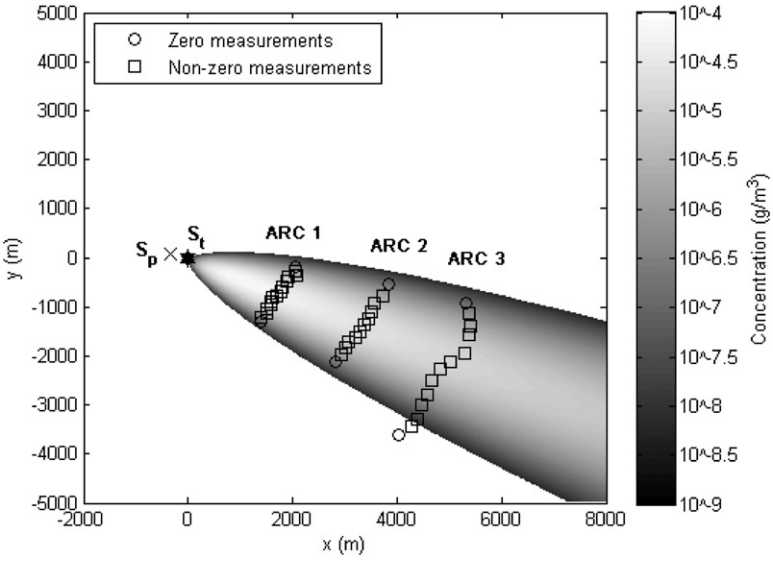

Figure 5. Plume spread predicted by model parameters from inversion. The squares (□) and the circles (○) represent sensors that recorded non-zero and zero measurements. 'S_t' (hexagon – ✱) is the true source location in, and 'S_p' (cross – ×) the location predicted by Newton's method.

The work of [9] used data from TCTE to demonstrate the Bayesian approach to solve the atmospheric inverse-source problem. The model parameters obtained from Newton's method cannot be directly compared to those obtained by [9] as [9] did not provide the expected values for the final model parameters. However, Figure 6 in their work shows the probabilistic plume spread for 95% confidence level. In Figure 5, the plume spread predicted by the parameters from Newton's method is shown. Comparing the figures it can be seen that the plume spread predicted by both the approaches has the same underlying characteristics in terms of the zero and non-zero measurements satisfied. Comparing Figure 5 with Figure 1 from this work, it can be seen that the plume spread predicted by parameters obtained from inversion matches the plume spread observed in TCTE better than the plume spread predicted by the true parameters.

The work of [20] also used the Copenhagen data for inversion. They employed a Langevin equation-based forward model and used the dataset recorded between 12 : 13 h and 12 : 33 h on 19 October 1978 (instead of the mean dataset, which is used in this work). To compare with the results of [20], the present approach is implemented with the dataset adopted by [20].

From Table 3 it can be seen that the predicted data from Newton's method matches 26 out of the 27 non-zero measurements, and 6 out of the 12 zero measurements, resulting in total number of matched measurements of 32 out of 39. In comparison, the predictions from [20] match all the non-zero measurements, but do not match any of the zero measurements, resulting in total matched measurements of 27 out of 39. Also, the values predicted by the present approach are closer to the observed data, than those predicted by [20]. The final model parameters predicted by Newton's method for the dataset between 12 : 13 h and 12 : 33 h are shown in Table 4. From Table 4 it is seen that using this dataset leads to improvement in inversion accuracy.

Downloaded by [University of Utah], [Michael Zhdanov] at 13:16 07 October 2011

Table 3. Comparison of the predicted concentrations from Newton's method with Copenhagen data (12 : 13 h–12 : 33 h on 19 October 1978) and [16].

Position	Sensor x-coordinate (m)	Sensor y-coordinate (m)	Observed concentration (ng m^{-3})	Predicted concentration [16] (ng m^{-3})	Predicted concentration from this work (ng m^{-3})
9	1398	−1312	0	721	0
10	1404	−1214	0	135	28
11	1492	−1131	186	2271	259.4
12	1516	−1044	614	3266	896
13	1582	−964	1816	4478	2672
14	1592	−884	5455	5105	4642.9
15	1602	−798	7016	5727	6682.1
16	1703	−767	6770	5582	7161.6
17	1766	−681	5472	5077	5860.7
18	1800	−593	3806	4067	3523.4
19	1877	−485	1114	2842	1053.1
20	1921	−405	919	1969	320.4
21	2067	−371	77	1902	101.6
22	2061	−284	0	1001	22.5
23	2055	−180	0	463	0
11	2818	−2134	0	1400	53.3
12	2920	−1987	107	1579	295.3
13	3002	−1830	840	2635	1022.3
14	3075	−1704	1478	2691	2029.3
15	3204	−1629	3133	2580	2797.2
17	3380	−1367	2563	2249	2627.3
18	3448	−1231	2225	2033	1614.8
19	3518	−1093	538	1282	722.2
20	3558	−919	0	1050	194.8
21	3729	−787	0	361	33.4
22	3837	−550	0	121	0
9	4027	−3616	0	306	0
10	4283	−3447	18	788	0
11	4390	−3277	21	1087	12.4
12	4459	−3010	85	1117	97.6
13	4572	−2795	800	1552	396.8
14	4668	−2514	1502	1236	1180.5
15	4824	−2260	2035	1297	1762.0
16	5029	−2108	1112	1063	1476.7
17	5286	−1939	434	778	761.8
18	5378	−1570	53	124	129.9
19	5395	−1399	0	49	42.1
20	5375	−1139	0	109	0
21	5323	−913	0	47	0

5.2. *Performance of the various QMC point-sets in the stochastic search stage*

The performance of the various QMC point-sets for SR1 and SR3 for the different N_S values described in Sections 4.3.2.1 (SR1) and 4.3.2.3 (SR3) is compared against the Mersenne–Twister pseudorandom generator. In the stochastic search stage, the number of

Downloaded by [University of Utah], [Michael Zhdanov] at 13:16 07 October 2011

Table 4. Computed inversion model parameters for TCTE using the dataset between 12 : 13 h and 12 : 33 h.

Model parameters	x_S (m)	y_S (m)	z_S (m)	q_S/u_S (gm^{-1})	θ_S (degrees)	N_S
m_t	0	0	115	0.64	308.57	–
$m_{STOCH+GD}$	64.001	2.58	181.49	1.11	295.11	32

Table 5. Performance of the various original QMC point-sets with SR1.

Point-sets	$N_S \geq 37$	$N_S \geq 38$	$N_S \geq 39$
E(MC)	12,633	82,102	25,000,000
O-Halton	6521	50,081	6666,989
O-Hammersley	678	17,730	4903,807
O-Sobol	1649	18,761	437,165
O-SplNie	24,377****	97,632****	1150,264
O-NieXing	10,040	159,266****	4434,687

Table 6. Performance of the various scrambled QMC point-sets with SR1.

Point-sets	$N_S \geq 37$	$N_S \geq 38$	$N_S \geq 39$
E(MC)	12,633	82,102	25,000,000
S-Halton	797	43,565	1740,461
S-Hammersley	2047	9250	–
S-Sobol	1230	23,758	1213,246
S-SplNie	29,265****	49,313	–
S-NieXing	6087	6087	2414,141

Table 7. Performance of the various original QMC point-sets with SR3.

Point-sets ($N_{S-NZ} = 34$)	$N_{S-Z} \geq 5$	$N_{S-Z} \geq 4$	$N_{S-Z} \geq 3$	$N_{S-Z} \geq 2$	$N_{S-Z} \geq 1$
E(MC)	25,000,000	114,943	32,342	12,533	9371
O-Halton	6666,989	50,081	50,081****	50,081****	50,081****
O-Hammersley	5258,175	–	4010	678	90
O-Sobol	437,165	18,761	1649	1649	1649
O-SplNie	1150,264	97,632	81,072****	10,224	10,224****
O-NieXing	–	171,000****	22,536	2240	2240

QMC points required to satisfy a given N_S value ($N_S = k$) was determined by the minimal number of points that satisfy $N_S \geq$ k. The results obtained are shown in Tables 5–8.

In Tables 5–8, *E*(MC) stands for the expected number of random samples required from the Mersenne–Twister generator to satisfy the given criteria. The letters *O* and *S*

Downloaded by [University of Utah], [Michael Zhdanov] at 13:16 07 October 2011

Table 8. Performance of the various scrambled QMC point-sets with SR3.

Point-sets ($N_{S-NZ} = 34$)	$N_{S-Z} \geq 5$	$N_{S-Z} \geq 4$	$N_{S-Z} \geq 3$	$N_{S-Z} \geq 2$	$N_{S-Z} \geq 1$
E(MC)	25,000,000	114,943	32,342	12,533	9371
S-Halton	18,025,133	188,933****	19,841	10,961	10,961
S-Hammersley	–	–	–	262	262
S-Sobol	–	23,758	1230	1230	1230
S-SplNie	–	49,313	29,265	10,609	9473****
S-NieXing	2414,141	6087	6087	4651	4651

before the various QMC point-sets are indicative of their original or scrambled nature. *SplNie* and *NieXing* are abbreviations for the SpecialNiederreiter and Niederreiter point-sets.

Based on the results obtained for SR1 and SR3 from Tables 5–8, the following conclusions can be made: (1) the QMC point-sets on average perform better then Mersenne–Twister generator for most of the cases, and (2) of all the QMC point-sets, the original Sobol sequence and the scrambled NiederreiterXing point-set perform better than the others (and the Mersenne–Twister generator).

The arguments based on which the original Sobol sequence and the scrambled NiederreiterXing point-set were determined to be the best of the point-sets considered are as follows: (1) The Hammersley point-set is not recommended as its first dimension is the regular 1D lattice evenly distributed on the interval [0, 1). Therefore, based on the number of points generated, the Hammersley sequence changes in the first dimension. Since the optimum number of points that should be generated for identifying the initial iterate with the fewest possible points is not known *a priori*, the Hammersley point-set is not recommended. Also, if the proposed approach is implemented with initial $\lambda = 90\%$ option, and if the λ value needs to be incremented subsequently, the entire simulation should be re-run if the Hammersley sequence is used. (2) Apart from the original Sobol and the scrambled NiederreiterXing point-sets, all other point-sets exceed the number of MC points required in at least one of the reported results in Tables 5–8. Such results are indicated either by the asterisk superscript (****), or have not been reported (indicated by ----) (whenever the number of QMC points required is much larger than *E*(MC)).

5.3. *Overall performance of the proposed approach*

The overall computational cost and thereby the execution time of the proposed approach can be divided between the stochastic and gradient stages. Depending on the strategy and the QMC point-set chosen in the stochastic stage, the computational costs and the execution times of the stochastic and the gradient stages vary. For TCTE, Newton's method always took less than 200 iterations irrespective of the strategy employed. The choice of SR1, SR2 and SR3 depends on the complexity of the problem at hand and on how much one is willing to expend on the stochastic search stage. To get an estimate for the execution time of the present approach, stochastic search was performed with the criteria, $N_S \geq 37$. Stochastic search was performed with the Mersenne–Twister generator, with the random number seed set to zero. With the initial iterate provided by the stochastic stage, 200 Newton iterations were run. The algorithm was implemented in 32-bit Matlab

Downloaded by [University of Utah], [Michael Zhdanov] at 13:16 07 October 2011

7.8.0 (R2009a) and was executed on a 64-bit Dell desktop machine running Windows Vista, with 8Gb RAM, and 3.0 GHz QuadCore processor. The overall execution time was ~3 s, with the stochastic stage taking ~2.3 s, and Newton's method taking ~0.7 s.

6. Conclusions

An inversion technique comprising stochastic search and regularized gradient optimization to solve the atmospheric inverse-source problem is described in this article. The inverse problem involves retrieving the spatial coordinates, source strength and the wind speed and wind direction at the source, given certain receptor locations and concentration values at these receptor locations. The GPM is adopted as the forward model and derivative-based optimization is chosen to take advantage of its simple analytical nature. The proposed approach is explained using the Copenhagen field experiment data. Stochastic search is performed over the domain of the misfit functional to identify an initial iterate for the gradient scheme. A new misfit functional is developed to take into account the zero and non-zero measurements recorded by the receptors and is used in the stochastic stage. It is based on the base 10 logarithm of the ratio of the observed and predicted data and it is shown that the new misfit functional improves the inversion accuracy. Several QMC point-sets in their original and scrambled forms are considered in the stochastic stage. Their performance are evaluated against the Mersenne–Twister generator. QMC point-sets are recommended for atmospheric inverse-source problems due to their deterministic and superior space-filling nature. Three strategies to solve the inverse-source problem are proposed and are implemented in the stochastic stage. The original Sobol and the scrambled NiederreiterXing point-sets are found to produce the best results across all the test cases considered. Newton's method with the Tikhonov stabilizer and adaptive regularization with quadratic line-search is implemented in the gradient stage. The final solution obtained from Newton's scheme is close to the true model parameters from the Copenhagen data.

References

[1] M.S. Zhdanov, *Geophysical Inverse Theory and Regularization Problems – Methods in Geochemistry and Geophysics*, Elsevier, Amsterdam, The Netherlands, 2002.
[2] Z.B. Zabinsky, *Stochastic Adaptive Search for Global Optimization*, Kluwer Academic, Dordrecht, The Netherlands, 2003.
[3] R. Sneider, *The role of nonlineaity in inverse problems*, Inverse Probl. 14 (1998), pp. 387–404.
[4] P.J. Ballester and J.N. Carter, *Characterizing the parameter space of a highly nonlinear inverse problem*, Inverse Probl. Sci. Eng. 14 (2006), pp. 171–191.
[5] B.L.N. Kennett, *Consistency regions in non-linear inversion*, Geophys. J. Int. 157 (2004), pp. 583–588.
[6] A. Lomax and R. Sneider, *Identifying sets of acceptable solutions to non-linear, geophysical inverse problems which have complicated misfit functions,* Nonlinear Processes Geophys. 2 (1995), pp. 222–227.
[7] M. Sambridge, *Finding acceptable solutions in nonlinear inverse problems using a neighbourhood algorithm*, Inverse Probl. 17 (2001), pp. 387–403.
[8] F. Chow, B. Kosovic, and S.T. Chan, *Source inversion for contaminant plume dispersion in urban environments using building-resolving simulations*, J. Appl. Meteorol. Climatol. 47 (2008), pp. 1553–1572.

Downloaded by [University of Utah], [Michael Zhdanov] at 13:16 07 October 2011

[9] I. Senocak, N.W. Hengartner, M.B. Short, and B.W. Daniel, *Stochastic event reconstruction of atmospheric contaminant dispersion using Bayesian inference*, Atmos. Environ. 42 (2008), pp. 7718–7727.
[10] V. Akecelik, G. Biros, A. Draganescu, O. Ghattas, J. Hill, and B.V.B. Waanders, *Lecture Notes on Computational Science*, International Conference on Computational Science, Reading, 2006.
[11] X. Davoine and M. Bocquet, *Inverse modelling-based reconstruction of the Chernobyl source term available for long-range transport*, Atmos. Chem. Phys. Discuss. 7 (2007), pp. 1–43.
[12] S. Houweling, T. Kamsinki, F. Dentener, J. Lelieveld, and M. Heimann, *Inverse modelling of methane sources and sinks using the adjoint of a global transport model*, J. Geophys. Res. 104 (1999), pp. 26137–26160.
[13] R.B. Storch, L.C.G. Pimentel, and H.R.B. Orlande, *Identification of atmospheric boundary layer parameters by inverse problem*, Atmos. Environ. 41 (2007), pp. 1417–1425.
[14] J.A. Scales and L. Tenorio, *Prior information and uncertainty in inverse problems*, Geophysics 66 (2001), pp. 389–397.
[15] S.E. Gryning and E. Lyck, *The Copenhagen tracer experiments: Reporting measurements*, Riso National Laboratory, Roskilde, 1998.
[16] A.J. Annunzio, S.E. Haupt, and G.S. Young, *Source Characterization and Meteorology Retrieval including Atmospheric Boundary Layer Depth using Genetic Algorithm*, 15th Joint Conference on the Applications of Air Pollution Meteorology with the A&WMA, New Orleans, LA, 2008.
[17] M.J. Brown, M.D. Williams, G.E. Streit, M. Nelson, and S. Linger, *An Operational Event Reconstruction Tool: Source Inversion for Biological Agent Detectors*, 86th American Meteorological Society Annual Meeting, 2006.
[18] S.E. Haupt, R.L. Haupt, and G.S. Young, *Using Genetic Algorithms in Chem-bio Defense Applications*, Proceedings of the 2007 ECSIS Symposium on Bio-inspired, Learning, and Intelligent Systems for Security, 2007.
[19] A. Khemka, C.A. Bouman, and M.R. Bell, *Inverse problems in atmospheric dispersion with randomly scattered sensors*, Digit. Signal Process. 16 (2006), pp. 638–651.
[20] K.J. Long, S.E. Haupt, G.S. Young, and C.T. Allen, *Characterizing Contaminant Source and Meteorological Forcing using Data Assimilation with a Genetic Algorithm*, 86th American Meteorological Society Annual Meeting, 2006.
[21] D.R. Roberti, D. Anfossi, H.F. de Campos Velho, and G.A. Degrazia, *Estimation of pollutant source emission rate from experimental data*, Il Nuovo Cimento 30 C(02) (2007), pp. 177–186.
[22] L.C. Thomson, B. Hirst, G. Gibson, S. Gillespie, P. Jonathan, K.D. Skeldon, and M.J. Padgett, *An improved algorithm for locating a gas source using inverse methods*, Atmos. Environ. 41 (2007), pp. 1128–1134.
[23] M.R. Beychok, *Fundamentals of Stack Gas Dispersion*, M.R. Beychok, Irvine, CA, 2005.
[24] B.D. Turner, *Workbook of Atmospheric Dispersion Estimates – An Introduction to Dispersion Modelling*, CRC Press, Boca Raton, FL, 1994.
[25] Y. Zhou and S.R. Hanna, *Along-wind dispersion of puffs released in a built-up urban area*, Boundary-Layer Meteorol. 125 (2007), pp. 469–486.
[26] R.I. Sykes, C.P. Cerasoli, and D.S. Henn, *The representation of dynamic flow effects in a Lagrangian puff dispersion model*, J. Hazardous Mater. 64 (1999), pp. 223–247.
[27] A. Trantola, *Inverse Problem Theory and Methods for Model Parameter Estimation*, SIAM, Philadelphia, PA, 2004.
[28] C.R. Vogel, *Computational Methods for Inverse Problems*, SIAM, Philadelphia, PA, 2002.
[29] D. Edwards, *Practical sampling for ray-based rendering,* Ph.D. diss., University of Utah, 2008.
[30] H. Niederreiter, *Random Number Generation and Quasi-Monte Carlo Methods,* CBMS-NSF Regional Conference Series in Applied Mathematics, 1992.
[31] J. Matousek, *On the L2-discrepancy for anchored boxes*, J. Complex. 14 (1998), pp. 527–556.
[32] R.C. Aster, B. Borchers, and C. Thurber, *Parameter Estimation and Inverse Problems*, Elsevier, Amsterdam, The Netherlands, 2005.

Downloaded by [University of Utah], [Michael Zhdanov] at 13:16 07 October 2011

[33] D. Zajic and M.J. Brown, *Source Inversion in Cities using the Collector Footprint Methodology,* 88th American Meteorological Society Annual Meeting, 2008.
[34] Anonymous, *Synopsis of the January 22-23, 2004 secretary's council on public health preparedness*, Biosecurity Bioterrorism: Biodefense Strat., Practice Sci. 2 (2004), pp. 41–45.
[35] C.T. Allen, S.E. Haupt, and G.S. Young, *Application of Genetic Algorithm-coupled Receptor/dispersion Model to the Dipole Pride 26 Experiments*, 14th Joint Conference on the Applications of Air Pollution Meteorology with the Air and Waste Management 2006.
[36] C.T. Allen, G.S. Young, and S.E. Haupt, *Improving pollutant source characterization by better estimating wind direction with a genetic algorithm*, Atmos. Environ. 41 (2007), pp. 2283–2289.
[37] J.V. Beck and K.A. Woodbury, *Inverse problems and parameter estimation: integration of measurement and analysis*, Meas. Sci. Technol. 9 (1998), pp. 839–847.
[38] M. Bocquet, *Reconstruction of an atmospheric tracer source using the principle of maximum entropy: I. Theory*, Q. J. R. Meteorol Soc. 131 (2005), pp. 2191–2208.
[39] M.N. Bradley, B. Kosovic, and J.S. Nasstrom, *Models and Measurements: Complementary Tools for Predicting Atmospheric Dispersion and Assessing the Consequences of Nuclear and Radiological Emergencies,* International Conference on Monitoring, Assessments, and Uncertainties for Nuclear and Radiological Emergency Response, 2005.
[40] P.E. Frandsen, K. Jonasson, H.B. Nielsen, and O. Tingleff, *Unconstrained Optimization,* Informatics and Mathematical Modelling, Technical University of Denmark.
[41] K.M. Hanson, *Quasi-Monte Carlo: Halftoning in high dimensions?*, Proc. SPIE 5016(1) (2003), pp. 161–172.
[42] S.E. Haupt and G.S. Young, *Paradigms for Source Characterization*, 88th American Meteorological Society Annual Meeting, 2008.
[43] W.R. Hogan, G.F. Cooper, M.M. Wagner, and G.L. Wallstrom, *An inversion Gaussian plume model for estimating the location and amount of release of airborne agents from downwind atmospheric concentrations,* The RODS laboratory, University of Pittsburgh.
[44] M.A. Islam, *Application of the Gaussian plume model to determine the location of an unknown emission source*, Water Air Soil Pollut. 112 (1999), pp. 241–245.
[45] C.T. Kelley, *Solving Nonlinear Equations with Newton's Method – Fundamentals of Algorithms*, SIAM, Philadelphia, PA, 1987.
[46] C. Lemieux, *Monte Carlo and Quasi-Monte Carlo Sampling*, Springer, New York, 2009.
[47] K. Mosegaard and A. Trantola, *Monte Carlo sampling of solutions to inverse problems*, J. Geophys. Res. 100 (1995), pp. 12431–12447.
[48] M. Sambridge, C. Beghein, F.J. Simons, and R. Sneider, *How do we understand and visualize uncertainty?*, Lead. Edge 25 (2006), pp. 542–546.
[49] M. Sambridge, *Inverse problems in a nutshell,* Center for Advanced Data Inference, Research School of Earth Sciences, Australian National University, ACT 0200, Australia.
[50] M. Sambridge and K. Mosegaard, *Monte Carlo methods in geophysical inverse problems*, Rev. Geophys. 40 (2002), pp. 1–29.
[51] A. Wirgin, *The inverse crime*, * LMA/CNRS, 31 chemin Joseph Aiguier, 13402 Marseille cedex 20, France.

Downloaded by [University of Utah], [Michael Zhdanov] at 13:16 07 October 2011